Fabrication, characterization, and theoretical analysis of controlled disorder in the core of optical fibers

Norma P. Puente,[1] Elena I. Chaikina,[2,*] Sumudu Herath,[3] and Alexey Yamilov[3,4]

[1]Facultad Ingenieria-Ensenada, Universidad Autonoma de Baja California, Ensenada, Baja California 22860, Mexico

[2]División de Física Aplicada, Centro de Investigación Científica y de Educación Superior de Ensenada, Ensenada, Baja California 22860, Mexico

[3]Department of Physics, Missouri University of Science & Technology, Rolla, Missouri 65409, USA

[4]yamilov@mst.edu

*Corresponding author: chaikina@cicese.mx

Received 5 October 2010; accepted 21 November 2010;
posted 7 January 2011 (Doc. ID 135726); published 11 February 2011

We present results of experimental and theoretical studies of polarization-resolved light transmission through optical fiber with disorder generated in its germanium-doped core via UV radiation transmitted through a diffuser. In samples longer than a certain characteristic length, the power transmitted with preserved polarization is observed to be distributed over all forward-propagating modes, as evidenced by the Rayleigh negative exponential distribution of the near-field intensity at the output surface of the fiber. Furthermore, the transmitted power becomes also equally distributed over both polarizations. To describe the optical properties of the fibers with the experimentally induced disorder, a theoretical model based on coupled-mode theory is developed. The obtained analytical expression for the correlation function describing spatial properties of the disorder shows that it is highly anisotropic. Our calculations demonstrate that this experimentally controllable anisotropy can lead to suppression of the radiative leakage of the propagating modes, so that intermode coupling becomes the dominant scattering process. The obtained theoretical expressions for the polarization-resolved transmission fit very well with the experimental data, and the information extracted from the fit shows that radiative leakage is indeed small. The reported technique provides an easy way to fabricate different configurations of controlled disorder in optical fibers suitable for such applications as random fiber lasers.

OCIS codes: 290.4210, 060.2310, 260.2160.

1. Introduction

In recent years, there has been a considerable interest in optical disordered media. This is largely due to the new functionalities brought about when disorder is introduced into homogeneous and periodic systems. A random laser [1], where laser action is ensured by coherent feedback in disordered structures such as powders or porous crystals, is a striking example. In Ref. [2], the advantages of disordered systems in wireless communications of high information capacity have been shown. It has also been reported [3] that the disorder induced in nonlinear crystals can greatly improve the efficiency of operation of nonlinear optical devices. It appears that disordered media open numerous possibilities for applications in sensors, nanophotonics, and, more generally, in various light transmission systems.

Localization of electromagnetic radiation in strongly disordered random media has attracted great interest from both fundamental and practical

0003-6935/11/060802-09$15.00/0

points of view [4]. Studied in the optical as well as in the microwave spectral regions, the phenomenon of localization depends on the dimensionality of the system. In particular, in surface- [5–7] and volume- [8] disordered waveguides, it leads to arbitrarily small transmission, which diminishes exponentially with the length of the system. This disorder-induced confinement can be employed in such an application as a laser.

Disorder-induced confinement has been shown to lead to unusual, while at the same time, useful properties in photonic-crystal waveguides [9] and in optical fibers [10–15]. An optical fiber is an extremely promising experimental system for random lasing applications [1]: Lizárraga *et al.* [15] reported coherent random lasing on randomly distributed Bragg gratings in single-mode optical fibers, whereas Turitsyn *et al.* [14] demonstrated an incoherent random lasing.

In this report we present experiments on the fabrication of random variations of the refractive index throughout the core of a Ge-doped multimode optical fiber, whose parameters can be controlled in our experimental setup. The characteristics of the disorder created are evaluated from an analysis of the intensity distribution of the near fields at the output of the fiber and by the analysis of the speckle size dependence of the total intensity of the transmitted light. The experimental results are compared and agreement is found, with the predictions of the coupled-mode theory, which is adapted to the particular type of volume disorder considered in this work. We show that by varying the correlation size of the disorder, scattering sufficiently strong for achieving the complete mixing of the forward-propagating modes can be achieved in a centimeter-length segment of multimode fiber. We also demonstrate that disorder with strongly anisotropic correlation function can lead to a dramatic suppression of radiative losses, so that coupling between modes becomes dominant. Thus, the scattering is much more efficient compared to the weak scattering of the material impurities as in, e. g., Ref. [14], and, unlike Bragg gratings, it is broadband in the propagation constant of a mode or the frequency of the light. The above properties of our system make it a promising candidate for fabrication of a compact multimode random fiber laser. This can be achieved by sandwiching the disordered segment of the fiber between two Bragg gratings, which would provide feedback.

The paper consists of the following sections. In Section 2, the experimental setup used for the fabrication of the fiber samples with disorder is described. In Section 3, we find the experimental and numerical results on the intensity distribution of light emerging from an optical fiber with different scales of the disorder. In Section 4, theoretical analysis of the optical properties of a fiber with speckled perturbations of the refractive index in its core is presented. Finally, discussion and outlook are presented in Section 5.

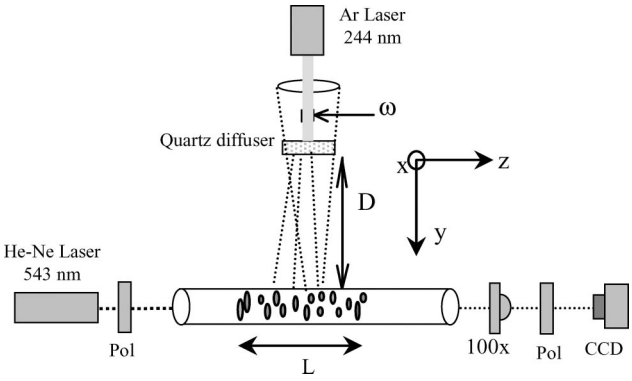

Fig. 1. Experimental setup.

2. Fabrication of the Disorder

The experimental setup utilized for the fabrication of disorder in optical fibers is schematically depicted in Fig. 1. In our experiments, we employed a step-index optical fiber (PS1250/1500 of Fibercore) sensitized by Ge. The main parameters of the fiber are a core diameter of 7.66 μm, cladding diameter of 125 μm, and numerical aperture (NA) of 0.13, with the refractive indices of the core and the cladding being 1.463 and 1.457, respectively. The cutoff wavelength of the fiber with these parameters is about 1200 nm. The disorder was introduced in the Ge-doped fiber core by exposing it to UV light from an intracavity frequency-doubled argon-ion laser (244 nm) that passed through a cylindrical lens and a diffuser, creating, in this way, a speckle pattern in a plane parallel to the fiber axis. The light beam generated by the UV laser was initially expanded by a cylindrical lens with a focal length of 12 cm in order to form an elliptical spot with desired dimensions at the diffuser plane. The beam transmitted through the diffuser was used for exposing the photosensitive fiber. Speckle, as the strongly fluctuating, grainy intensity pattern resulting from the interference of randomly scattered coherent waves, resulted in fluctuations of the illuminating UV intensity in the fiber core. An expression for the size of a speckle, Eqs. (6)–(8) is derived in Section 4 below. It depends on the distance between the diffuser and the fiber axis, D, the size of the illuminated region in the diffuser plane $L_{x,z}$, and the wavelength of the recording UV light λ_{UV}. Variations of D in the range 2–8 mm and of $L_{x,z}$ in the range of 8–10 mm allowed us to obtain an average speckle size along the fiber axis between 200 and 600 nm.

The length of each segment with the fabricated disorder was 1–2 mm. The experimental geometry allowed us to record the segments with lengths up to 5 cm. In order to achieve disorder with similar statistical parameters in each segment, the same exposure time was used for all segments, namely, about 10 min at a mean power of the UV laser of about 100 mW. We observed experimentally that after this exposure, the intensity distribution of the output probe light at the fiber output did not change. Every next segment with a random distribution of the

refractive index was recorded directly after the preceding one. The total lengths of the fabricated disordered part (L_s) were 2, 4, 6, 8, 10, and 15 cm.

After forming the disordered segment, we launched the probe beam of the He–Ne laser operated at $\lambda = 543$ nm into the fiber, and detected the image of the output intensity distribution by a CCD camera (ST-402ME SBIG). The selected wavelength 543 nm of the probe beam ensured a low mode-number propagation regime, and corresponded to the sensitivity range of the CCD camera quite well. The light emerging from the fiber passed through the microscope objective ×100, which imaged the output end of the fiber on the CCD camera. In front of the CCD camera there was a polarizer utilized for characterization of the transmitted light.

3. Experimental Results

The resulting V parameter of the utilized fibers was 5.8171 at the probe wavelength, and the expected number of the guided LP modes is $N = 20$. By varying the angle of incidence of the probe beam, different combinations of modes were excited and the corresponding near-field transmitted intensity was recorded. It appears that these measurements can be made quite reliably. Indeed, (i) the light polarization was preserved in the straight fiber without disorder and (ii) the ambient temperature was controlled by a special air conditioning system that excluded the fluctuation of the parameters of the fiber samples during measurements. At the input of the optical fiber, the polarized light goes through a half-wave plate and a linear polarizer. The output light was detected separately for both polarizations: (i) after passing through a polarizer of the same orientation as at the input (pp polarization) or (ii) perpendicularly polarized (ps polarization). We analyzed the output light of each polarization independently. The polarization extinction ratio of the laser source and the fiber output was measured in the linear transmission regime.

Examples of the intensity distribution of the light emerging from the fiber, obtained for different realizations of the disorder and for different angles of the incident beam with disordered segments of the fiber of 1 (a) and 2 cm (b) length, are presented in Fig. 2. The left column presents results of pp-polarization measurements, and the right column presents results of ps-polarization measurements. Different realizations were obtained by slightly bending the disordered part of the fiber.

In Fig. 3, the ensemble-averaged intensities of the output light measured experimentally as functions of the length of the disordered parts of the fiber are presented. The averaging was performed over ten realizations. The solid and dashed curves are the fit with the theoretical expression Eqs. (24) and (25) obtained from Eq. (19) in the Section 4. The theoretical and experimental results show excellent agreement.

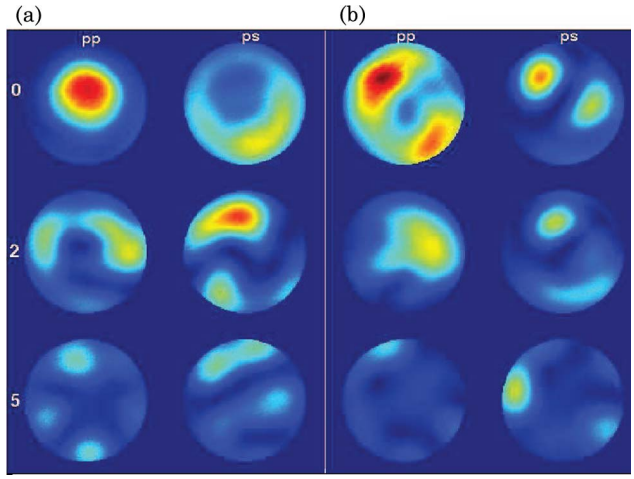

Fig. 2. (Color online) Examples of the output intensity distribution observed in some realizations with the disordered part of fiber (a) 1 cm and (b) 2 cm. The left column in each figure presents the pp-polarized distribution, and the right column presents the ps-polarized distribution. The angles of incidence are 0°, 2°, and 5° from the top to the bottom images.

4. Coupled-Mode Theory in Fibers with Speckled Perturbations of the Refractive Index

As was shown in Section 3, the random fluctuations of the refractive index imprinted in the core of the photosensitive fiber resulted in the mixing of different forward-propagating modes. To describe this process and to obtain the characteristic (mixing) length of the disordered segment of fiber, we employ the coupled-power method developed by Marcuse [16]. However, because the disorder induced by the speckle pattern (see Section 3) does not allow a factorization of the refractive index modulations into a product of a function of the transverse coordinates

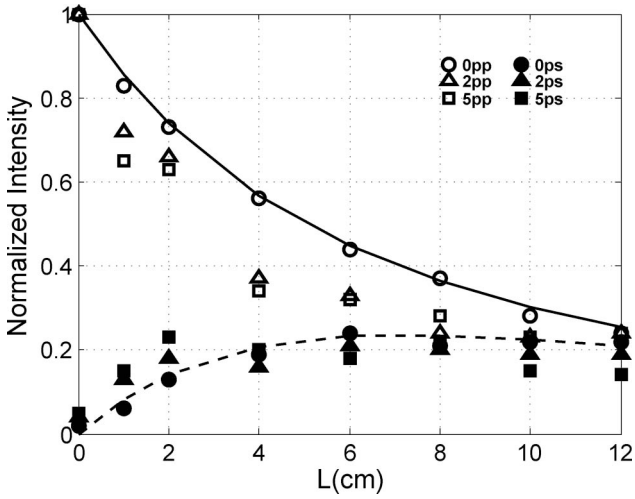

Fig. 3. Experimentally measured total co- (open symbols) and cross-polarized (solid symbols) transmission as a function of the length of the disordered part of the fiber for different polarizations of the transmitted beam. The circles correspond to an angle of incidence of 0°, the triangles to 2°, and the squares to 5°. Solid and dashed curves represent the theoretical fit with Eqs. (24) and (25) with parameters $\alpha = 0.064\,\mathrm{cm}^{-1}$, $\sigma_2 = 0.1917\,\mathrm{cm}^{-1}$.

and a function of the longitudinal coordinate $\delta n(x,y,z) \neq \delta n(x,y) \times f(z)$, the original derivation is not applicable. The goal of this section is to obtain a system of coupled-power equations applicable to the experimentally induced disorder. In the process of derivation we verify that coupling between the forward and backward propagating modes is negligible. We also give detailed estimates of the radiative loss due to scattering into the nonguiding modes. We show that because of the highly asymmetric correlation function of the disorder, the radiative loss is greatly reduced, so it becomes comparable to the coupling coefficients between guided modes.

A. Statistical Properties of the Disorder

To begin our analysis, we need to obtain the statistical properties of the disorder, specifically, the two-point correlator of the fluctuations of the dielectric function $\langle \delta\varepsilon(\mathbf{r})\delta\varepsilon(\mathbf{r}')\rangle$, where the angular brackets denote averaging over different realizations of disorder. Here we defined the fluctuation of the dielectric function $\delta\varepsilon(\mathbf{r}) = \varepsilon(\mathbf{r}) - \langle\varepsilon(\mathbf{r})\rangle$, which has the property $\langle\delta\varepsilon(\mathbf{r})\rangle = 0$. We make an assumption that in the process of exposure to the ultraviolet (UV) radiation, the material in the fiber core remains in a linear regime, i.e.,

$$\langle \delta\varepsilon(\mathbf{r})\delta\varepsilon(\mathbf{r}')\rangle = \langle\delta\varepsilon^2\rangle \frac{|\langle \mathbf{A}(\mathbf{r})\mathbf{A}^*(\mathbf{r}')\rangle|^2}{\langle|\mathbf{A}(\mathbf{r})|^2\rangle\langle|\mathbf{A}(\mathbf{r}')|^2\rangle} \equiv \langle\delta\varepsilon^2\rangle|\mu(\mathbf{r}',\mathbf{r})|^2, \tag{1}$$

where $\mathbf{A}(\mathbf{r})$ are statistically uniform complex field amplitudes of the UV light scattered by the diffuser. The amplitudes can be computed in the paraxial approximation with the help of the Fresnel diffraction integral, which propagates the fields delta-correlated in the plane of the diffuser; the procedure is described in Subsection 4.D of Ref. [17]. In our problem, we are interested in $\langle \delta\varepsilon(\mathbf{r})\delta\varepsilon(\mathbf{r}')\rangle$ as a function of all three spatial coordinates, including both those perpendicular (x and z axes) and parallel (y axis) to the direction of the UV illumination. In the geometry considered, it is impossible to obtain such an expression in a compact form. To proceed, we assume that

$$\mu(\mathbf{r}',\mathbf{r}) \approx \mu(\mathbf{r}'-\mathbf{r}) \approx \mu(x-x',0,z-z')\mu(0,y-y',0). \tag{2}$$

In this expression the first factor describes the correlation in the plane perpendicular to the UV propagation, whereas the second factor describes the depth of the speckle. The expressions for these functions can now be computed with the knowledge that the Gaussian UV laser beam is spread out by the cylindrical lens to cover the spot

$$I(\tilde{x},\tilde{z}) \propto \exp[-\tilde{x}^2/L_x^2 - \tilde{z}^2/L_z^2], \tag{3}$$

where $\tilde{x}$, $\tilde{z}$ denote the coordinates in the plane of the diffuser. The intensity distribution in Eq. (3) allows one to compute the Fresnel integrals [17], which define the correlation functions $\mu(x-x',0,z-z')$ and $\mu(0,y-y',0)$ in Eq. (2). Performing the integrations, we obtain

$$|\mu(x-x',0,z-z')|^2 = \exp\left[-\left(\frac{x-x'}{S_x}\right)^2\right] \times \exp\left[-\left(\frac{z-z'}{S_z}\right)^2\right], \tag{4}$$

$$|\mu(0,y-y',0)|^2 = \frac{1}{\left(1+\left[\frac{\pi L_x^2}{\lambda_{\mathrm{UV}}D^2}(y-y')\right]^2\right)^{1/2}\left(1+\left[\frac{\pi L_z^2}{\lambda_{\mathrm{UV}}D^2}(y-y')\right]^2\right)^{1/2}} \approx \frac{1}{\left(1+\left[\frac{y-y'}{S_y^2}\right]^2\right)^{1/2}}. \tag{5}$$

The length S_i was introduced to describe the spatial dimensions of the speckles:

$$S_x = \frac{\lambda_{\mathrm{UV}}D}{\sqrt{2}\pi n_{\mathrm{core}}L_x} \approx 0.15\frac{\lambda_{\mathrm{UV}}D}{L_x}, \tag{6}$$

$$S_y = \frac{\sqrt{3}\lambda_{\mathrm{UV}}D^2}{\pi n_{\mathrm{core}}L_z^2} \approx 0.38\frac{\lambda_{\mathrm{UV}}D^2}{L_z^2}, \tag{7}$$

$$S_z = \frac{\lambda_{\mathrm{UV}}D}{\sqrt{2}\pi n_{\mathrm{core}}L_z} \approx 0.15\frac{\lambda_{\mathrm{UV}}D}{L_z}, \tag{8}$$

where D denotes the distance from the diffuser to the fiber core during the exposure; all dimensions are scaled by the refractive index of the core; and $L_z \gg L_x$ is assumed in Eq. (5). Finally, by substituting Eqs. (4) and (5) into Eq. (1), we obtain the desired expression for the second-order statistics of disorder introduced in imprinting the speckle pattern in the core of the photosensitive optical fiber:

$$\langle \delta\varepsilon(\mathbf{r})\delta\varepsilon(\mathbf{r}')\rangle \approx \langle\delta\varepsilon^2\rangle \exp\left[-\left(\frac{x-x'}{S_x}\right)^2\right] \frac{1}{\left[1+\left(\frac{y-y'}{S_y^2}\right)^2\right]^{1/2}} \times \exp\left[-\left(\frac{z-z'}{S_z}\right)^2\right]. \tag{9}$$

The parameter $\langle\delta\varepsilon^2\rangle = 2n_{\mathrm{core}}\Delta n_{\mathrm{UV}}$ is related to the change in the refractive index Δn_{UV} due to the UV irradiation. We note that the above approximate expression remains valid for $|y-y'| \leq S_y$. For $|y-y'| \gg S_y$ the factor omitted in Eq. (5) has to be also included to ensure that the function is normalizable.

B. Derivation of Coupled-Power Equations

We begin our derivation of a system of coupled-power equations by expressing the electric field in terms of the linearly x- and y-polarized modes in the weakly guiding step-index fiber without disorder:

$$\mathbf{E}(\mathbf{r}) \approx \sum_{\nu} c_{\nu}(z) e^{i(\omega t - \beta_{\nu} z)} (\mathcal{E}_{t,\nu}(x,y) + \hat{e}_z \mathcal{E}_{z,\nu}(x,y)). \quad (10)$$

Here the summation runs over all modes ν of the fiber, including the odd and even modes of both x (odd ν's) and y polarizations (even ν's), assumed to be normalized as

$$\beta_{\nu} \iint [\mathcal{E}_{t,\nu}(x,y) \cdot \mathcal{E}_{t,\nu'}(x,y)] \mathrm{d}x\mathrm{d}y = \delta_{\nu\nu'}, \quad (11)$$

where $\delta_{\nu\nu'}$ is the Kronecker symbol. Equation (10) contains contributions from only forward-propagating modes. In Subsection 4.C we will support this assumption by showing that the coupling coefficients into the backpropagating modes is negligible.

Further, in Eq. (10) both the transverse $\mathcal{E}_{t,\nu}(x,y)$ and the longitudinal $\hat{e}_z \mathcal{E}_{z,\nu}(x,y)$ components of the individual modes are retained despite the smallness of the latter. As will be seen below, retaining the longitudinal components is crucial because it gives the dominant contribution to the coupling between the modes with the orthogonal polarizations. β_{ν} is the propagation constant of the νth mode, and $c_{\nu}(z)$ is its amplitude at position z along the fiber.

Following [16], we obtain the coupled amplitude equation

$$\frac{dc_{\nu}(z)}{dz} = \sum_{\nu'} \mathcal{K}_{\nu\nu'}(z) c_{\nu'}(z) e^{i(\beta_{\nu} - \beta_{\nu'})z}, \quad (12)$$

where

$$\mathcal{K}_{\nu\nu'}(z) = \frac{\omega^2}{2c^2} \iint \delta\varepsilon(\mathbf{r}) [\mathcal{E}_{t,\nu}(x,y) \cdot \mathcal{E}_{t,\nu'}(x,y) + \mathcal{E}_{z,\nu}(x,y) \mathcal{E}_{z,\nu'}(x,y)] \mathrm{d}x\mathrm{d}y \quad (13)$$

are the amplitude coupling coefficients. The system of equations Eq. (12) can be used to obtain the solution for a particular realization of the random function $\delta\varepsilon(\mathbf{r})$. The ensemble-averaged information can be obtained by defining the power in each mode as $P_{\nu} = \langle |c_{\nu}|^2 \rangle$, which satisfies the evolution equation:

$$\frac{dP_{\nu}}{dz} = \left\langle c_{\nu}^* \frac{dc_{\nu}}{dz} \right\rangle + \text{c.c.}, \quad (14)$$

where c.c. stands for the complex conjugate. We proceed by substituting Eqs. (12) and (13) into Eq. (14). Evaluation of the ensemble average $\langle \ldots \rangle$ requires the following two assumptions. $P_{\nu}(z)$ is assumed to vary on scales much larger than that of the disorder $S_z \sim \lambda$. This assumption is easily satisfied because the magnitude of the refractive index fluctuations is small—$\Delta n_{\mathrm{UV}} \ll 1$. The experimental data in Fig. 3 further corroborate this assertion.

At this point, our derivation departs from that of Marcuse [16]. To evaluate $\langle |\mathcal{K}_{\nu\nu'}(z)|^2 \rangle$, instead of the stringent requirement that the function describing the disorder in the refractive index can be factorized as $\delta n(x,y,z) \neq \delta n(x,y) \times f(z)$, we use a much weaker assumption that z dependence is factorizable in $\langle \delta\varepsilon(\mathbf{r}) \delta\varepsilon(\mathbf{r}') \rangle$. Indeed, the multiplicative property of the correlation in the speckle in Eq. (9) that separates the dependencies on the transverse (x and y) and the longitudinal (z) coordinates, enables one to complete the derivation of the system of coupled-power equations

$$\frac{dP_{\nu}}{dz} = \sum_{\nu'} h_{\nu\nu'} (P_{\nu'} - P_{\nu}), \quad (15)$$

with the power coupling coefficients given by the following expression

$$h_{\nu\nu'} = \langle \delta\varepsilon^2 \rangle \frac{\omega^4 \pi \log(2) S_x S_y S_z}{c^4} e^{-S_z^2 |\beta_{\nu} - \beta_{\nu'}|^2/4} \times \iint [\mathcal{E}_{t,\nu}(x,y) \cdot \mathcal{E}_{t,\nu'}(x,y) + \mathcal{E}_{z,\nu}(x,y) \mathcal{E}_{z,\nu'}(x,y)]^2 \mathrm{d}x\mathrm{d}y. \quad (16)$$

In obtaining Eq. (16) we approximated $\exp[-(x-x')^2/S_x^2] \times [1 + (y-y')^2/S_y^2]^{-1/2}$ by the product of two delta functions $4\pi^{1/2} \log(2) S_x S_y \delta(x-x') \delta(y-y')$ with the coefficients chosen so that both pairs of functions enclose identical area. This approximation is justified fairly well in our case because $S_{x,y}$ are smaller than the characteristic scale, a, of the field variation in the transverse direction for all guided modes. In case of the function that describes y dependence, the full expression Eq. (5) was used to obtain the normalization, and the correction terms logarithmic in L_x/L_z were omitted in the result.

C. Efficiency of Backscattering

In the process of derivation of the coupled power equations, Eqs. (15) and (16), we neglected the possibility of scattering from a forward-propagating mode into one of the backward-propagating modes. This is an important process which, if efficient, can give rise to the phenomenon of Anderson localization, which originates in the studies of mesoscopic systems in condensed matter physics [18]. Multiple scattering and interference of the forward- and backward-propagating waves can suppress transmission and lead to an exponential decay of the transmission coefficient. This dependence may appear similar to that observed in Fig. 3.

To estimate the efficiency of the backscattering process in our system, we compute the forward-to-backward coupling coefficients. The derivation

follows the steps similar to those in Subsection 4.B, with the final expression for $h_{\nu\nu'}^{+,-}$ being given by the formula similar to Eq. (16) with an exception that the $\exp[-S_z^2|\beta_\nu - \beta_{\nu'}|^2/4] \simeq 1$ factor is replaced by $\exp[-S_z^2|\beta_\nu + \beta_{\nu'}|^2/4] \ll 1$. One can see that this difference proves to be extremely important because $|\beta_\nu - \beta_{\nu'}| \ll |\beta_\nu + \beta_{\nu'}| \simeq 2n_{\text{core}} \times (2\pi/\lambda)$ and $S_z \lesssim \lambda$ in our fibers.

The above estimate shows that the backscattering mechanism is, indeed, strongly suppressed in the considered system as it was assumed in the previous section. As a consequence, we do not expect our system to exhibit the phenomenon of Anderson localization.

D. Radiative Losses

Optical fiber with unwanted or purposefully introduced, as in our case, modulations of the refractive index are invariably susceptible to the radiative losses. Indeed, the index nonuniformity couples the modes guided in the core of the fiber to the nonguided modes that extend into the cladding and are effectively lost. Even the fibers of the highest quality suffer from radiative loss from Rayleigh scattering on molecular inclusions introduced in its fabrication process [19]. The consequence of this loss is the exponential decay of the power in a mode $P_\nu(z) \propto \exp[-\alpha_\nu z]$. Unlike the losses suffered in waveguides with rough surfaces, the radiative loss in the volume-disordered fibers, such as fibers with molecular defects, should not exhibit a strong dependence on the mode index ν. Because the fibers studied in this work are of the latter kind, we will assume $\alpha_\nu \equiv \alpha$ hereafter.

In Chap. 4 of Ref. [16], Marcuse has derived an expression for α in the case of Rayleigh scattering. It is interesting to note that under quite general conditions, the ratio between coupling coefficients and the scattering loss appears to be independent of the disorder parameters [20]

$$\frac{\alpha}{h_{\nu\nu'}} \simeq \frac{2}{3\pi} k_0^2 n_{\text{core}}^2 A, \tag{17}$$

where $k_0 = 2\pi/\lambda$ and A is the area of the fiber core. One can easily see that the above estimate gives $\alpha/h_{\nu\nu'} \gg 1$ for a step-index fiber with $(n_{\text{core}} - n_{\text{cladding}})/n_{\text{core}} \ll 1$. Evaluating this ratio for our system gives a number on the order of a thousand. Although the above estimate is made under the assumption of Rayleigh scattering, it may still be applicable in our case. This is because the Rayleigh criterion involves not only the smallness of the scatterer compared to the wavelength of light but also the difference between its refractive index and that of the surrounding [21]. Below, we expose a flaw in this logic and show that Eq. (17) is not applicable to our system and that, instead, $\alpha \sim h_{\nu\nu'}$

Unlike a deterministic scattering off a single particle, the scattering in a random system has to properly account for the exact autocorrelation function given in our system by Eq. (9). The combined effect for a group of scatters can be greatly diminished if the phases of the partial waves are sufficiently random. Quantitatively, this effect is described [16] by the following integral

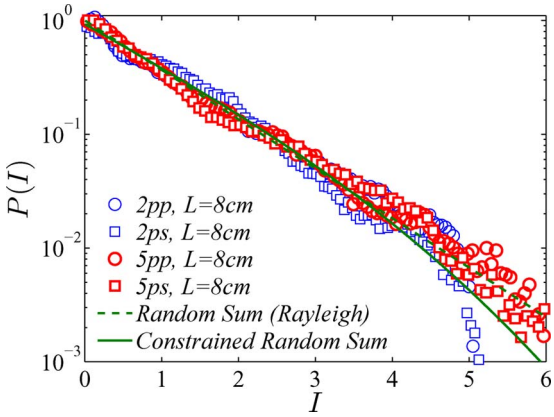

Fig. 4. (Color online) The distributions, which correspond to an unconstrained random sum (shown as a dashed curve) and to a constrained random sum (shown with the solid curve) of all modes of the fiber, are compared to the experimentally observed distributions of the near-field intensity measured in co- (circles) and cross-polarized (squares) channels in a sample with $L = 8$ cm. The thin symbols correspond to an angle of incidence of 2°, and the bold symbols correspond to an angle of incidence of 5°.

$$\alpha \propto I = \int d\Omega_{\Delta\mathbf{k}} (\hat{\boldsymbol{e}}_{\text{scat}} \cdot \hat{\boldsymbol{e}}_z)^2 \iiint_{-\infty}^{\infty} du_x du_y du_z \langle \delta\varepsilon(\mathbf{r}) \delta\varepsilon(\mathbf{r}+\mathbf{u}) \rangle \times \exp[i\Delta\mathbf{k} \cdot \mathbf{u}]. \tag{18}$$

Here, $\Delta\mathbf{k} \approx n_{\text{core}} k_0 (\hat{\boldsymbol{e}}_{\text{scat}} - \hat{\boldsymbol{e}}_z)$ defines the change of wavevector after scattering and $\int d\Omega_{\Delta\mathbf{k}} \ldots$ denotes the solid angle integration over all possible scattering directions.

The Rayleigh approximation in Eq. (18) amounts to assuming that disorder is correlated in the volume L_{corr}^3 much less than λ^3, which results in $\exp[i\Delta\mathbf{k} \cdot \mathbf{u}] \simeq 1$. In the optical fibers with photoinduced disorder considered in our work, this assumption is no longer valid. Thus, the Rayleigh result $I = (4\pi/3)\langle \delta\varepsilon^2 \rangle L_{\text{corr}}^3$ needs to be reevaluated for the correlator Eq. (9) we obtained in Subsection 4.A.

Calculation of the triple integral in Eq. (18) is facilitated by the fact that $\langle \delta\varepsilon(\mathbf{r}) \delta\varepsilon(\mathbf{r}+\mathbf{u}) \rangle$ is factorizable into three functions, each of which depend only on one spatial variable. The integrals over u_x and u_z give rise to $\sqrt{\pi} S_{x,z} \exp[-(\Delta k_{x,z} S_{x,z}/2)^2]$. The integral over u_y does not give, in general, a compact expression. However, in a special case when $L_x = L_z$, it leads to a simple expression that illuminates the general tendency: $\pi S_y \exp[-\Delta k_y S_y]$. Inspection of all three integrals shows that the result of the triple integral in Eq. (18) is a function that is very strongly peaked around $|\Delta\mathbf{k}| = 0$. Therefore, the remaining integration over solid angles should produce a result much smaller than $4\pi/3$ predicted for the isotropic (Rayleigh) scattering. To complete our calculation

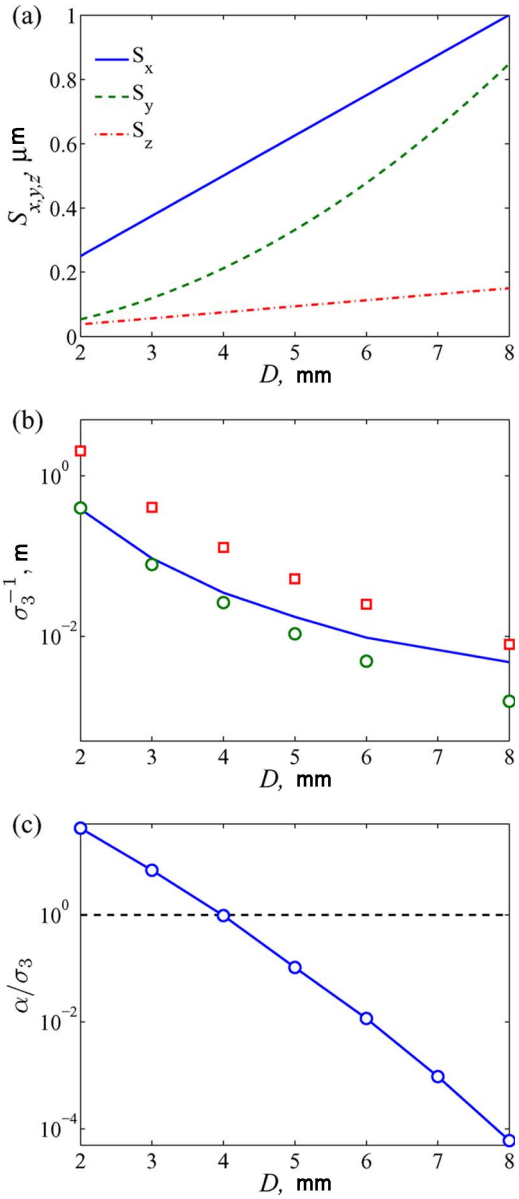

Fig. 5. (Color online) Panel (a) plots the size of the speckle defined by Eqs. (6)–(8) with $L_x = 0.3\,\mathrm{mm}$ and $L_z = 2\,\mathrm{mm}$ as a function of the distance between the diffuser and the core of the photosensitive fiber. Panel (b) compares the values of the characteristic length $\ell^{(xx)-1} \equiv \sigma_3$ after which all forward-propagating modes with one polarization become equally populated. It is found numerically from Eq. (16) without (solid curve) and with (circles) the delta function approximation to the order of magnitude estimate (squares) in Eq. (29). Panel (c) compares the amplitude of the radiative loss rate computed from Eq. (18) to the intermode coupling rate σ_3. The plot shows that for the disorder patterns generated with $D > 4\,\mathrm{mm}$, the coupling becomes the dominant effect. This conclusion is borne out by the experimental results in Fig. 3.

of the absorption coefficient α we perform the integral over $d\Omega$ in Eq. (18) numerically and report the results in Fig. 5.

E. Solution of Coupled-Power Equations

The system of coupled-power Eqs. (15) obtained in Subsection 4.B did not account for loss. This omission can be rectified by a phenomenological correction due Marcuse [16]

$$\frac{dP_\nu}{dz} = -\alpha P_\nu + \sum_{\nu'} h_{\nu\nu'}(P_{\nu'} - P_\nu). \tag{19}$$

Such a treatment of loss can be rigorously justified in the case when the such a loss is independent of the mode index [22]. As already mentioned in the preceding section, this is a reasonable assumption for the volume-disordered fibers that we also adopt here.

Solution of Eqs. (19) proceeds with two steps. First, the effect of the radiative loss is factored out with substitution

$$P_\nu(z) = P_\nu^{(\mathrm{lossless})}(z) \times \exp[-\alpha z], \tag{20}$$

which reduces Eqs. (19) back to Eqs. (15) satisfied now by $P_\nu^{(\mathrm{lossless})}(z)$.

In the second step, the solution for $P_\nu^{(\mathrm{lossless})}(z)$ is obtained by the following ansatz

$$P_\nu^{(\mathrm{lossless})}(z) = A_\nu \exp[-\sigma z], \tag{21}$$

where σ_n and the corresponding set of $A_\nu^{(n)}$ are to be determined by substitution of Eq. (21) into Eq. (15). Here σ_n are the eigenvalues of the secular equation

$$\det\left[h_{\nu\nu'} - \delta_{\nu\nu'}\sum_\tau h_{\nu\tau} + \sigma\right] = 0, \tag{22}$$

arranged in increasing order. The overall solution for $P_\nu(z)$ takes the form

$$P_\nu(z) = e^{-\alpha z} \times \left[\sum_n c_n A_\nu^{(n)} e^{-\sigma_n z}\right],$$
$$\text{with } c_n = \left[\sum_n A_\nu^{(n)} P_\nu(0)\right]. \tag{23}$$

Because the effect of radiative loss has been factored out in Eq. (20), the conservation of the total power for $P_\nu^{(\mathrm{lossless})}$ requires $\sigma_1 \equiv 0$ and, subsequently, $A_\nu^{(1)} = \mathrm{const} = 1/N$ leads to uniform distribution of the power over all modes. The knowledge of σ_n allows estimation of the characteristic lengths of the disordered region of the fiber beyond which such an asymptotic state is achieved, $\ell^{(xx)} \equiv \sigma_3^{-1}$, and for cross-polarized modes, $\ell^{(xy)} \equiv \sigma_2^{-1}$. Assuming that the fiber is excited with some mode combination (with total input power equal to unity) of the same polarization, which we assume to be x for definiteness, and recalling mode numbering convention in Eq. (10), we obtain

$$P^{(x)}(z) \equiv \sum_{\nu=0}^{N/2-1} P_{2\nu+1} \approx e^{-\alpha z} \times \frac{1}{2}[1 + e^{-\sigma_2 z}], \tag{24}$$

$$P^{(y)}(z) \equiv \sum_{\nu=1}^{N/2} P_{2\nu} \approx e^{-\alpha z} \times \frac{1}{2}[1 - e^{-\sigma_2 z}]. \qquad (25)$$

The above equations have the following properties. Without loss and polarization coupling, $P^{(x)}(z) = 1$ reflects power conservation. In the presence of absorption $P^{(x)}(z) + P^{(y)}(z) = \exp[-\alpha z]$ exhibits attenuation due to the radiative losses.

In the case when coupling between two orthogonal subsets of LP modes of the fiber is weak, $\sigma_2 \ll \alpha \ll \sigma_3$, Eq. (23) yields $P^{(y)}(z) \sim 0$, $P^{(x)}(z) \simeq \exp[-\alpha z]$ and the system reaches the state when the power is equally distributed only over $(N/2)$ modes with initially excited polarization, x:

$$P_{2\nu+1}(z) \approx e^{-\alpha z} \times \left[\left(P_{2\nu+1}(0) - \frac{2}{N}\right)e^{-\sigma_3 z} + \frac{2}{N}\right],$$
$$P_{2\nu}(z) \sim 0. \qquad (26)$$

The above analysis shows that the redistribution of the power carried by the forward-propagating modes can be detected by making the following observations:

- Making polarization-resolved measurement of the light intensity at the output surface of the fiber and averaging it over several disorder configurations should show that the intensity profile approaches the limit. Alternatively, the conclusion that a perfect mixing (in a statistical sense, i.e., $P_\nu(z \to \infty) \to$ const) indeed occurs in our experimental system can also be tested through measurements of the distribution of the near-field intensity at different spatial locations for just one realization of disorder. A random sum of different modes of the fiber $\sum_\nu c_\nu \mathcal{E}_{t,\nu}(x,y)$ with $P_\nu \approx$ const is expected [17] to result in the Rayleigh negative exponential distribution of the intensity. In an optical fiber, however, the coefficients c_ν are not completely random because the total power carried by all modes is constrained by $\sum_\nu |c_\nu(z)|^2 = \exp[-\alpha z]$. This constraint, similar to the power conservation in the lossless fibers [23], makes the distribution deviate slightly from the Rayleigh form. As we can see from Fig. 4, the agreement between theory and experiment is very good, whereas the level of precision of the experimental data does not allow distinguishing between the two theoretical functions—unconstrained and constrained random sums of all modes of the fiber.
- The dependence of $P^{(x)}(z = L_s), P^{(y)}(z = L_s)$ on the length of the disordered segment of the fiber, L_s, is expected to be described by Eqs. (24) and (25). We observe that the power carried by a particular mode ν, $P_\nu = \beta_\nu \iint [\mathcal{E}_{t,\nu}(x,y) \cdot \mathcal{E}_{t,\nu'}(x,y)]\mathrm{d}x\mathrm{d}y$ is equal to the product of nearly ν-independent $\beta_\nu \approx n_1 k_0$ and the field intensity integrated over the surface of the fiber $\mathcal{I}$. Therefore, even in the case of superposition of several modes with the same polarization, the area-integrated intensity at the output facet $\mathcal{I}^{(x,y)} = \iint |\sum_\nu c_\nu \mathcal{E}_{t,\nu}^{(x,y)}(x,y)|^2 \mathrm{d}x\mathrm{d}y = \sum_\nu \iint |c_\nu|^2 |\mathcal{E}_{t,\nu}^{(x,y)}(x,y)|^2 \mathrm{d}x\mathrm{d}y \approx (1/n_1 k_0)\sum_\nu P_\nu^{(x,y)}$ is proportional to $P^{(x)}(z)$ and $P^{(y)}(z)$ given by Eqs. (24) and (25). The outcome of the fit by these expressions to the experimental data in Fig. 3 allows one to extract the characteristic mixing length $\ell^{(xy)} = \sigma_2^{-1}$ and loss coefficient α.

Approximate expressions for the mixing lengths can be obtained in a compact analytic form by taking into account the fact that both the transverse $\mathcal{E}_{t,\nu}(x,y)$ and the longitudinal $\hat{e}_z \mathcal{E}_{z,\nu}(x,y)$ modal profiles are spread out over the entire core of the fiber. This observation together with Eq. (11) allows one to estimate

$$\iint [\mathcal{E}_{t,\nu}(x,y) \cdot \mathcal{E}_{t,\nu'}(x,y) + \mathcal{E}_{z,\nu}(x,y)\mathcal{E}_{z,\nu'}(x,y)]^2 \mathrm{d}x\mathrm{d}y, \quad (27)$$

$$\approx \begin{cases} [n_{\mathrm{core}}^2(\omega^2/c^2)\pi a^2]^{-1} & xx, yy \\ (\mathrm{NA}/2)^4 [n_{\mathrm{core}}^2(\omega^2/c^2)\pi a^2]^{-1} & xy, yx \end{cases}. \qquad (28)$$

where a is the radius of the fiber core. In the second case of the cross-polarized modes, we also used the fact that the amplitude of the $\mathcal{E}_{z,\nu}(x,y)$ component is a factor NA/2 smaller compared to the amplitude of the transverse fields. The approximations in Eq. (28), $\sigma_{2,3} \sim h_{22,33}$ and $S_z|\beta_\nu - \beta_{\nu'}| \ll 1$ allow us to obtain our final result in a closed analytical form

$$\ell^{(xx)-1} \equiv \sigma_3 \sim \frac{\Delta n}{2n_{\mathrm{core}}} \frac{\pi\omega^2 S_x S_y S_z}{c^2 a^2} = \frac{\Delta n}{n_{\mathrm{core}}^4} \frac{\lambda_{\mathrm{UV}}^3 D^4}{\lambda^2 a^2 L_x L_z^3},$$
$$\ell^{(xy)-1} \equiv \sigma_2 \sim \ell_{\mathrm{mixing}}^{(xx)-1} \left(\frac{\mathrm{NA}}{2}\right)^4, \qquad (29)$$

where Eqs. (6)–(8) were used.

In Fig. 5(a) we plot the dependence of the speckle size as a function of the distance D between the diffuser and the fiber core. It is clear that tuning this parameter allows one to widely tune the characteristic size of the prepared disorder. This is an attractive feature of the fabrication technique described in Section 2.

In Fig. 5(b) three expressions for $\ell^{(xx)}$ obtained in this section are compared. As expected, for a small speckle size (small D), the approximation of Eq. (9) by a product of delta functions appears to be justified and gives a quite accurate result when compared to the direct numerical evaluation of $h_{\nu\nu'}$.

Numerical evaluation of the exact expressions in Eq. (16) and (22) with the experimentally relevant parameters ($L_x = 0.5\,\mathrm{mm}$, $L_z = 3\,\mathrm{mm}$ and $D = 0.5\,\mathrm{cm}$) yields $\sigma_3 = \ell^{(xx)-1} \simeq 0.15\,\mathrm{cm}^{-1}$, $\sigma_2 = \ell^{(xy)-1} \simeq 3 \times 10^{-6}\,\mathrm{cm}^{-1}$, and $\alpha \simeq 0.015\,\mathrm{cm}^{-1}$.

5. Conclusion

We have studied the transmission of light through a volume-disordered multimode optical fiber. The disorder was introduced in the germanium-doped core

of the fiber via UV radiation transmitted through a diffuser. The disorder generated in an optical fiber can be controlled by the experimental conditions, and it is determined by the speckle size and the value of the induced difference in the refractive index. The measurement of the transmission as a function of the length of the disordered section demonstrates the uniform distribution of the power over all forward-propagating modes beyond $L_s = 15\,\mathrm{cm}$. For long sections of a disordered fiber, the experimentally measured distribution of the near-field intensity at the output surface of the fiber is well described by the Rayleigh negative exponential function. The presented technique provides an easy way to fabricate different configurations of controlled disorder in optical fibers suitable for applications as a coherent and incoherent random fiber laser. Although the specific type of disorder studied in our work leads to mixing of only forward-propagating modes, the feedback necessary to produce laser action can be achieved by surrounding the disordered fiber with Bragg gratings.

Analysis of Fig. 3 shows that the power transfer into the cross-polarized modes occurs quite efficiently with $\ell^{(xy)} \simeq \ell^{(xx)}$. This differs from the predictions of the coupled-mode theory developed in Section 4 that gives $\ell^{(xy)} \gg \ell^{(xx)}$. We attribute this enhanced cross polarization coupling to the (i) birefringence effect induced by the bending of the fiber, and (ii) strongly anisotropic disorder pattern defined by Eq. (9). Indeed, although no polarization mixing is observed in the blank fibers (before the disorder is introduced), to generate the statistical ensemble of different realization, the 30 cm long fiber sample was displaced in the lateral directions, while both of the sample's ends were fixed by fiber clips. As a result of fiber bending and tension, a pronounced birefringence was induced. For our experimental condition, we estimate the minimum radius of the bending as 250 cm, which gives birefringence of $\Delta n \sim 4 \times 10^{-5}$ [24]. Formally, the induced birefringence enables coupling via the transverse components of the modes' field that is expected to remove the small factor $(\mathrm{NA}/2)^4$, which leads to the $\ell^{(xy)} \gg \ell^{(xx)}$ condition in Eq. (28). The effect of induced birefringence will be reported in a separate publication.

We thank A. A. Maradudin and E. R. Méndez for stimulating discussions and constructive comments to the manuscript. N. P. Puente and E. I. Chaikina would like to acknowledge support by Consejo Nacional de Ciencia y Tecnología (Mexico), under grant UCM-42127. The work at Missouri University of Science & Technology was supported by the University of Missouri Research Board and by National Science Foundation grant DMR-0704981.

References

1. H. Cao, "Review on latest developments in random lasers with coherent feedback," J. Phys. A **38**, 10497–10535 (2005).
2. S. H. Simon, A. L. Moustakas, M. Stoytchev, and H. Safar, "Communication in a disordered world," Phys. Today **54**(9), 38–43 (2001).
3. S. E. Skipetrov, "Disorder is the new order," Nature **432**, 285–286 (2004).
4. A. Lagendijk, B. van Tiggelen, and D. Wiersma, "Fifty years of Anderson localization," Phys. Today **62**(8), 24–29 (2009).
5. J. A. Sánchez-Gil, V. D. Freilikher, A. A. Maradudin, and I. Yurkevich, "Reflection and transmission of waves in surface disordered waveguides," Phys. Rev. B **59**, 5915–5925 (1999).
6. E. I. Chaikina, S. Stepanov, A. G. Navarrete, E. R. Méndez, and T. A. Leskova, "Formation of angular power profile via ballistic light transport in multi-mode optical fiber with corrugated surface," Phys. Rev. B **71**, 085419 (2005).
7. F. Bass, V. Freilikher, and I. Fuks, "Propagation in statistically irregular waveguides—part I: average field," IEEE Trans. Antennas Propagat. **22**, 278–288 (1974).
8. A. A. Chabanov, M. Stoytchev, and A. Z. Genack, "Statistical signatures of photon localization," Nature **404**, 850–853 (2000).
9. J. Topolancik, F. Vollmer, and B. Ilic, "Random high-*Q* cavities in disordered photonic crystal waveguides," Appl. Phys. Lett. **91**, 201102 (2007).
10. O. Shapira and B. Fischer, "Localization of light in a random-grating array in a single-mode fiber," J. Opt. Soc. Am. B **22**, 2542–2552 (2005).
11. C. Lu, J. Cui, and Y. Cui, "Reflection spectra of fiber Bragg gratings with random fluctuations," Opt. Fiber Technol. **14**, 97–101 (2008).
12. C. J. S. Matos, L. de S. Menezes, A. M. Brito-Silva, M. A. Martinez-Gámez, A. S. L. Gomes, and C. B. de Araújo, "Random laser action in the core of a photonic crystal fiber," Opt. Photon. News **19**(12), 27–27 (2008).
13. M. Gagné and R. Kashyap, "Demonstration of a 3 mW threshold Er-doped random fiber laser based on a unique fiber Bragg grating," Opt. Express **17**, 19067–19074 (2009).
14. S. K. Turitsyn, S. A. Babin, A. E. El-Taher, P. Harper, D. V. Churkin, S. I. Kablukov, J. D. Ania-Castñón, V. Karalekas, and E. V. Podivilov, "Random distributed feedback fibre laser," Nature Photon. **4**, 231–235 (2010).
15. N. Lizárraga, N. P. Puente, E. I. Chaikina, T. A. Leskova, and E. R. Méndez, "Single-mode Er-doped fiber random laser with distributed Bragg grating feedback," Opt. Express **17**, 395–404 (2009).
16. D. Marcuse, *Theory of Dielectric Optical Waveguides* (Academic, 1974).
17. J. W. Goodman, *Speckle Phenomena in Optics: Theory and Applications* (Roberts, 2007).
18. P. W. Anderson, "Absence of diffusion in certain random lattices," Phys. Rev. **109**, 1492–1505 (1958).
19. D. Marcuse, "Rayleigh scattering and the impulse response of optical fiber," Bell Syst. Tech. J. **53**, 705–715 (1974).
20. B. Crosignani, A. Saar, and A. Yariv, "Coherent backscattering and localization in a single-mode fiber with random imperfections," Phys. Rev. A **43**, 3168–3171 (1991).
21. H. C. van de Hulst, *Light Scattering by Small Particles* (Dover, 1981).
22. D. Marcuse, "Coupled power equations for lossy fibers," Appl. Opt. **17**, 3232–3237 (1978).
23. J. C. Dainty, "Recent developments," in *Laser Speckle and Related Phenomena*, J. C. Dainty, ed. (Springer, 1984).
24. Luc B. Jeunhomme, *Single-Mode Fiber Optics* (Marcel Dekker, 1990).